ACS SENSORS

pubs.acs.org/acssensors

Article

Resettable Microfluidics for Broad-Range and Prolonged Sweat Rate Sensing

Mallika Bariya,[#] Noelle Davis,[#] Liam Gillan, Elina Jansson, Annukka Kokkonen, Colm McCaffrey, Jussi Hiltunen, and Ali Javey*

Cite This: *ACS Sens.* 2022, 7, 1156–1164

Read Online

ACCESS | Metrics & More | Article Recommendations | Supporting Information

ABSTRACT: Wearable sweat sensors are emerging as promising platforms for personalized and real-time tracking of evolving health and fitness parameters. While most wearable sweat sensors focus on tracking biomarker concentration profiles, sweat secretion rate is a key metric with broad implications for assessing hydration, cardiac, and neural conditions. Here we present a wearable microfluidic sensor for continuous sweat rate measurement. A discrete impedimetric sensing scheme relying on interdigitated electrodes within a microfluidic sweat collector allows for precise and selective sweat rate measurement across a broad physiological range. Integration of a manually activated pressure pump to expel sweat from the device prevents sensor saturation and enables continuous sweat rate tracking over hours. By enabling broad range and prolonged sweat rate measurement, this platform tackles a key obstacle to realizing meaningful and actionable sweat sensing for applications in exercise physiology and medicine.

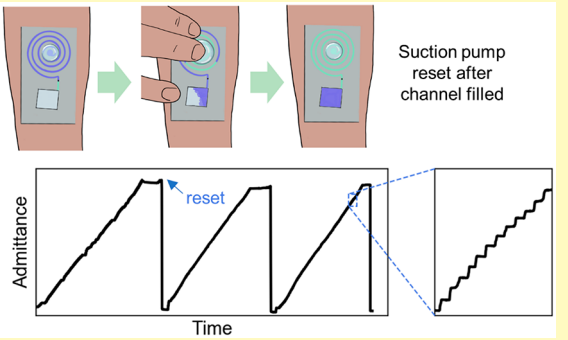

KEYWORDS: *sweat sensor, sweat rate, continuous monitoring, wearable electronics, flexible sensor, printed electronics*

Human sweat has been shown to provide valuable insight on underlying body function.[1−5] While recent sweat analysis wearables have focused primarily on measuring biomarker concentrations,[6−18] one of the most physiologically informative parameters is the sweat secretion rate. Sweat rate is important to track as it modulates the concentrations of secreted analytes,[5] but even as a standalone, it can indicate evolving or unfavorable health conditions including cardiac complications, neural damage,[2,19] response to physical or emotional stimuli,[20,21] and dehydration.[1,22,23] During exercise, local sweat rate measured on the forearm or another convenient location has been shown to correlate with whole-body sweat volume loss,[24,25] creating opportunities for tracking hydration status in real time.[26−28] Precise and continuous sweat rate measurement is therefore an important component of wearable sweat sensing technology.[29]

Sweat rate is measured clinically to diagnose hyperhidrosis, a condition that causes excessive sweating, for which iodine-starch tests are used. This method involves coating the skin with a chemical that changes color upon interaction with water. Quick color change over broad areas of the skin surface indicate rapid sweat secretion and suggest hyperhidrosis. However, this method has limitations as it is not very quantitative. Other methods include using gravimetric pads to weigh secreted sweat or affixing humidity chambers to the skin surface. These methods are limited by evaporation errors and a lack of portability, underscoring the need for wearable, autonomous sweat rate measurement systems. One method that has shown promise for real-time monitoring of local sweat rate involves collecting sweat in a wearable microfluidic collector and tracking the progression of the advancing fluid front using embedded electrodes.[25,30,31] This scheme enables autonomous, electrical measurements of the sweat rate that have advantages over visual schemes of tracking sweat accumulation within a device.[32−34] The changing impedance electrically measured between the electrodes can be converted into real-time sweat rate data. However, a key limitation of this approach is that it is volume-limited: continued, updated sweat rate measurement is not possible once the microfluidic channel has filled with sweat and the electrode admittance saturates. Other approaches that similarly rely on detecting the changing volume of captured sweat within a microchannel face the same volume limitation for the duration that the sweat rate can be accurately tracked.[24,35] For example, optical sweat rate measurements utilize colored dye or channel functionalization to track the flow of sweat through a microfluidic channel at discrete time points.[24] Capacitive measurements rely on the

Received: January 21, 2022
Accepted: April 1, 2022
Published: April 12, 2022

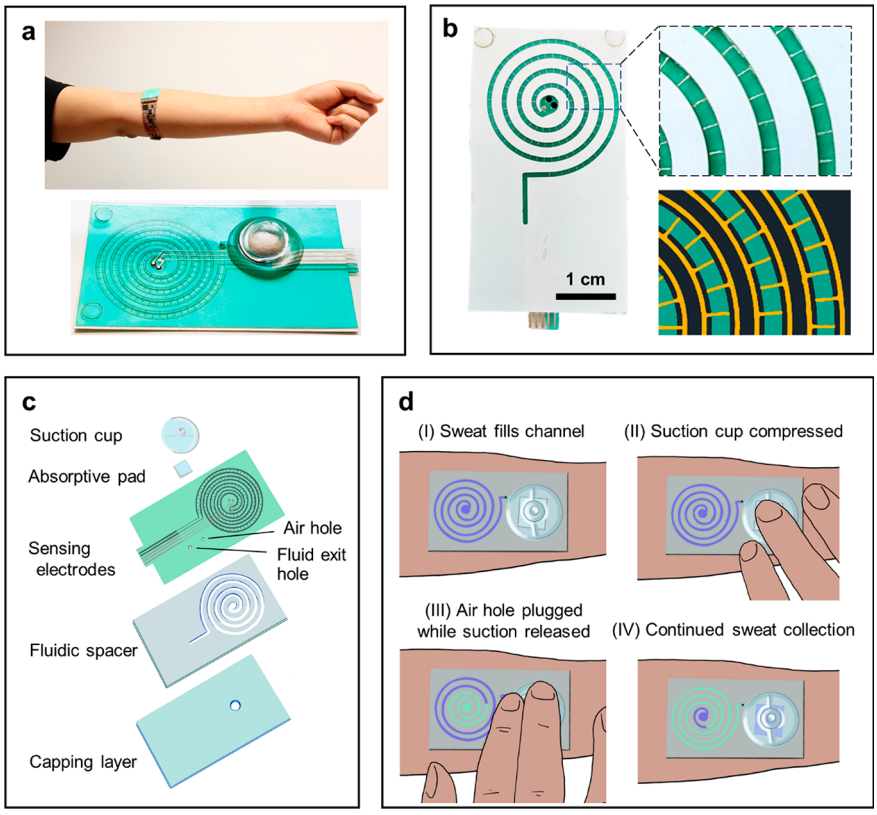

Figure 1. (a) Microfluidic patch with negative pressure reset shown in conformal on-body wear with wireless readout system as standalone. (b) Design of interdigitated flow rate electrodes reaching across the microfluidic channel. In the illustration, the channel is shown in green and electrodes in gold. (c) Stack of device layers including capping layer with inlet hole against the skin, microfluidic spacer, and sensing electrode layer with outlet holes. The reset mechanism is on top, including absorptive pad and suction cup. (d) Reset actuation in four steps.

significantly higher dielectric strength of aqueous solutions over air, resulting in a measurably higher capacitance across the microchannel as sweat flows through.[35] In both cases, updated sweat rate tracking ends once the sweat collecting channel is filled.

This volume limitation of common sweat rate measurement techniques in wearable sensors greatly restricts the applicability of these devices for real-world monitoring. For instance, consider a wearable microfluidic sweat collector previously reported for exercise sweat rate sensing, with a 4 cm^2 footprint and sweat collection area, and a sweat collecting channel of 24 μL volume.[25] At a typical exercise-induced sweat rate of 0.75 $\mu L\ min^{-1}\ cm^{-2}$ on the forearm, where a typical sweat gland density is 150 glands cm^{-2},[5] the microfluidic channel would fill and sweat rate measurements would cease after a mere 8 min.[4,5] This short duration limits the utility of such a patch, as it cannot measure the sweat rate for long enough to capture physiologically significant changes in the hydration state without requiring the wearer to replace the patch with a fresh one multiple times per hour. In effect, this short measurement capability renders the sensor ineffective as an autonomous system for routine use.

A cursory approach to solving this problem is to shrink the microfluidic patch collection area to proportionately scale down the volume and rate of collected sweat, enabling slower accumulation into the microchannel's fixed volume and therefore longer measurement times. However, the collection area is limited by local sweat gland densities and must remain large enough to target several sweat glands simultaneously to generate sufficient pressure for sweat to push into the microfluidic device, and to ensure that variations in individual gland secretion behavior do not cause misleading irregularities in the overall measured sweat flow. Targeting on the order of 50 sweat glands requires about 0.3 cm^2 of skin surface on common body sites, posing a rough lower limit on the size of the sweat collection well and the volumetric flow rate within the device.[28] An alternate route to overcoming the volume limitation is to increase the footprint of the patch so that it supports a longer microfluidic channel length. However, the device footprint must be consolidated enough that it stays locally flat on the body's curvilinear surface in order to avoid device delamination and maintain close, conformal body contact. This constrains the total channel length and volume, especially for the more curved body sites popular for wearable sweat sensing such as the wrists, arms, and forehead.

In this work, we present a strategy to enable continuous, prolonged sweat rate sensing by integrating a reset capability to expel collected sweat from the device once the channel is filled. In this way, the impedance between electrodes embedded within the channel is reset for continued impedimetric sweat rate measurement. We demonstrate this wearable patch during a range of mild to strenuous physical activity with continuous monitoring of sweat rate over 10 h. This extended capability for sweat rate tracking makes this device uniquely appropriate for health tracking during high sweat rate and prolonged physical activity, which is crucial for detecting and potentially avoiding adverse physiological conditions like dehydration. Working toward precise, long-duration sweat rate monitoring will enhance the value of sweat sensing beyond the lab toward important applications in exercise, wellness, and medicine.

https://doi.org/10.1021/acssensors.2c00177
ACS Sens. 2022, 7, 1156−1164

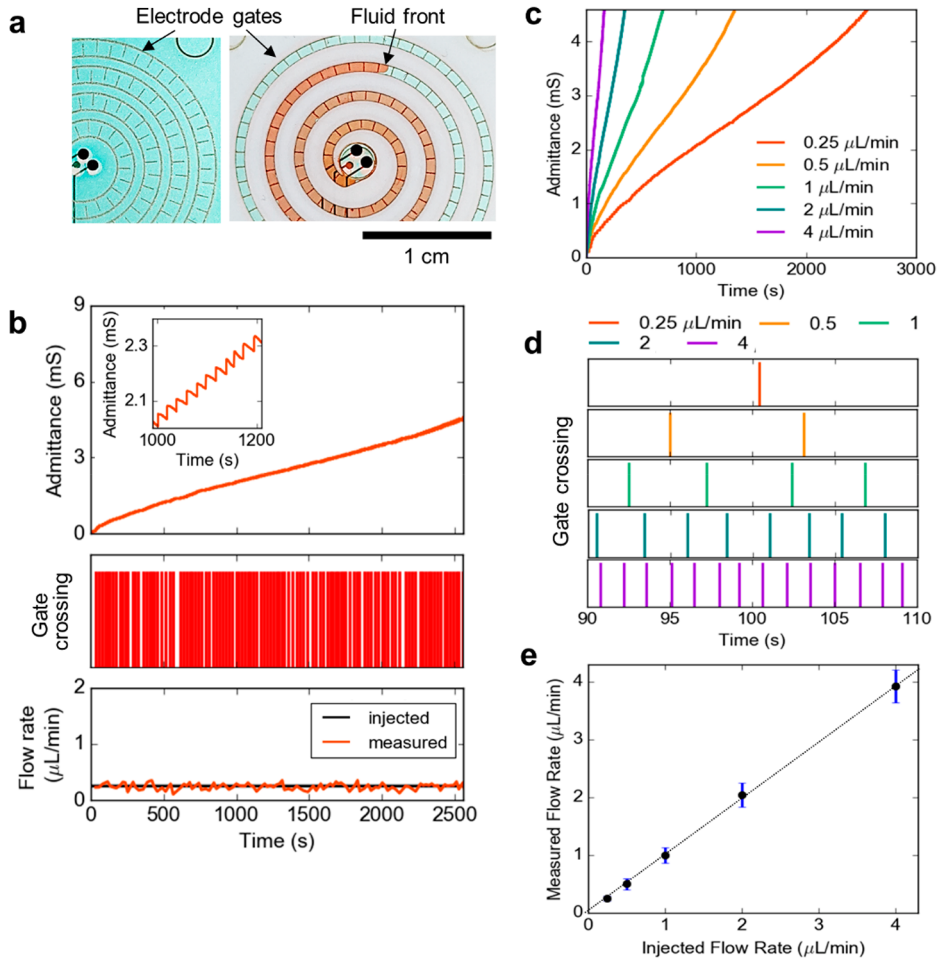

Figure 2. Sweat rate sensor calibration and method of sweat rate reconstruction from admittance measurements. (a) Buffer solution dyed red for visualization is injected into the microfluidic channel and the flow rate is measured. (b) Controlled flow at 0.25 μL min^{-1} is injected and reconstructed. (c) The device is used to measure a range of flow rates from 0.25 to 4 μL min^{-1}. (d) True/false determination of gate crossing occurrences is shown for a shorter window of time. The time between a pair of adjacent gate crossings is converted to a discrete flow rate measurement. (e) Individual flow rate measurements have high fidelity to the true injected flow rate, even with some error from the peristaltic flow pump itself. Mean and standard deviation of discrete measurements during a single fill of a device (n = 148) are plotted for each tested flow rate.

RESULTS AND DISCUSSION

The resettable sweat rate sensor, shown in Figure 1, is designed to enable robust sweat rate measurement during prolonged, strenuous exercise and is manufactured using high-throughput roll-to-roll (R2R) technologies to produce devices at scale with low variability.[36,37] It consists of a microfluidic channel with embedded flow rate electrodes and a polydimethylsiloxane (PDMS) reset button. The device comes together as a series of mass-produced layers (Figure 1c) that can be rapidly assembled, including a laser-cut spacer layer to define a channel and a hydrophilic polyester layer that seals the channel on one side and has a 9 mm^2 circular inlet hole for sweat entry from the skin surface. Sealing the other side of the microchannel is a polyethylene terephthalate (PET) layer with R2R rotary screen-printed electrodes that make contact with sweat in the channel for impedimetric sweat rate tracking. Sweat enters the channel at the center of the patch and flows outward in the spiraling microchannel toward an exit hole from which it can be expelled. The device channel is 86 μm high, 700 μm wide, and 170 mm long to support an overall volume of 10 μL before resetting must be actuated for continued measurement. At the center of the patch, a PDMS button sits over an additional hole in the PET layer to force fluid out of the channel when manually activated. Two reset mechanisms—negative and positive pressure—were developed and are shown in Figure 1d and SI Figure 2, respectively. These mechanisms will be discussed in more detail in the following sections.

Sweat Rate Measurement. The flow rate measurement is performed by two disjoint comb-like electrodes with backbones located just outside the spiraling fluid channel and interdigitated spokes that protrude into the channel (Figures 1b, 2a). Fluid traveling through the channel does not contact the electrode backbones, but crosses their spokes in alternating order. This sensing structure advances on previous demonstrations of impedimetric sweat rate sensing. For example, a previously demonstrated architecture monitored the continuous change in admittance between parallel electrodes spiraling within the microchannel, but suffered from selectivity limitations as the admittance was impacted by changing ionic composition of accumulating sweat, preventing selective sweat volume or rate measurement.[25] Instead, in the device presented here, discrete changes in admittance between the interdigitated, protruding electrodes spokes are monitored rather than the continuous admittance changes that would occur if the spiraling backbones were directly immersed in

https://doi.org/10.1021/acssensors.2c00177
ACS Sens. 2022, 7, 1156−1164

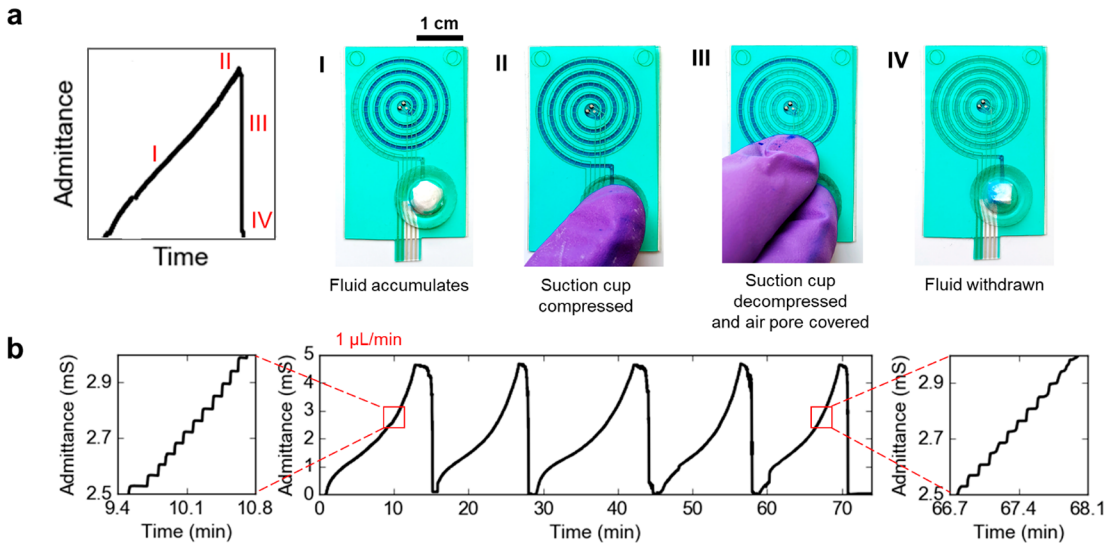

Figure 3. Negative pressure suction reset for continuous and repeatable flow rate measurement with dyed buffer solution. (a) (I) After sweat fills the 10 μL microfluidic channel, the patch is reset. (II) First, one finger is used to compress the suction cup, located above the fluid exit hole. The displaced air flows out of the adjacent air exchange hole, which must then (III) be covered for the released suction cup to generate a negative pressure in the channel and (IV) withdraw the column of fluid. (b) Corresponding admittance curve steps up to ~5 mS during each fill of the channel and falls back to zero when the fluid is expelled.

sweat. These discrete admittance changes, or steps, occur when sweat accumulating and advancing in the channel bridges the next protruding electrode spoke, forming a sudden additional electrical connection between the electrode backbones and creating an overall admittance signal that uniquely depends on the position of the sweat front within the channel (Figure 2b). The exact magnitude of the admittance step is inconsequential, but it is set by the ionic composition of the sweat, as seen in SI Figure 5. Specifically, step size is set by the oldest captured sweat, which constitutes the front of the sweat column that is flowing in the channel and making new connections between electrode gates, with some effects from diffusion in the channel. With the slow pace of physiological sweat ion changes, occurring no more quickly than the span of minutes,[38] dramatic changes in admittance that occur over seconds can definitively be ascribed to a new electrode gate being crossed. Because the regular spacing of electrode spokes defines a preset volume increment between them, each admittance step corresponds to that additional, incremental volume of sweat being added into the channel. Therefore, the number of admittance steps detected over time can be accurately translated into a volumetric sweat flow rate. Electrode spokes are situated at 1.2 mm intervals along the channel for a 72 nL volumetric resolution, enabling close tracking of sweat rates on the order of 1 μL cm^{-2} min^{-1}, sweat rates that are typical on body sites like the forearm during exercise.[5]

Admittance step rate is identified by continuously measuring admittance between the embedded electrodes and first detecting when sudden increases occur, signifying where a spoke has been crossed as shown in Figure 2b. As these steps occur uniquely when sweat has reached known positions within the channel, namely, where the electrode spokes have been patterned at regular intervals, the volumetric increment between these gates can be divided by the time between the admittance jumps to quantify sweat rate (Figure 2c). A higher flow rate is indicated by a higher frequency of gate crossings, as shown in Figure 2d. This measurement scheme is demonstrated for five different flow rates between 0.25 and 4 μL min^{-1}, encompassing a broad range of physiological sweat rates that can be obtained from 2 cm^2 collection area. Fluid is delivered into the device at each set constant rate using an injection pump, and the flow rate in the device is measured via the scheme detailed above to simulate on-body sweat rate measurement. Mean and standard deviation of the measured flow rate from a device filling at each rate are shown in Figure 2e, demonstrating high accuracy across a range of physiologically relevant flow rates, with error values much smaller than the measurement for each test case. This calibration acts to verify sensor performance and accuracy given the lack of accurate, quantitative, and practical standards of sweat rate measurement.

Sweat Withdrawal and Channel Reset. As presented so far, a limitation of this discrete, spiraling sweat rate sensing architecture is that the sweat rate measurement can only continue as long as there is still available empty volume along the microchannel for the accumulating sweat front to advance into. Once the microchannel is filled, the admittance response plateaus. New sweat can continue to enter the device via gland-originated pressure,[5] pushing old sweat out of the exit hole at the end of the microchannel, but the rate of secretion can no longer be tracked. This limitation is shared by the continuous impedimetric, colorimetric, and capacitive sweat rate sensing schemes discussed previously.[24,25,30,35] Enhancing the volumetric capacity by increasing channel length is limited by the requirement of conformal device-to-skin contact; at the same time, widening the channel cross-sectional area would cause the sweat front to move slowly through the channel, increasing the time between each electrode gate crossing and limiting how frequently sweat rate measurements can be made. A narrow channel and an overall compact patch footprint are desirable but limit the volume capacity of the microfluidic.

A solution to this limitation is to introduce resettability into the 10 μL sensing patch, whereby accumulated sweat can be periodically expelled from the device to make room for fresh sweat to newly cover the sweat rate electrode gates and allow

https://doi.org/10.1021/acssensors.2c00177
ACS Sens. 2022, 7, 1156−1164

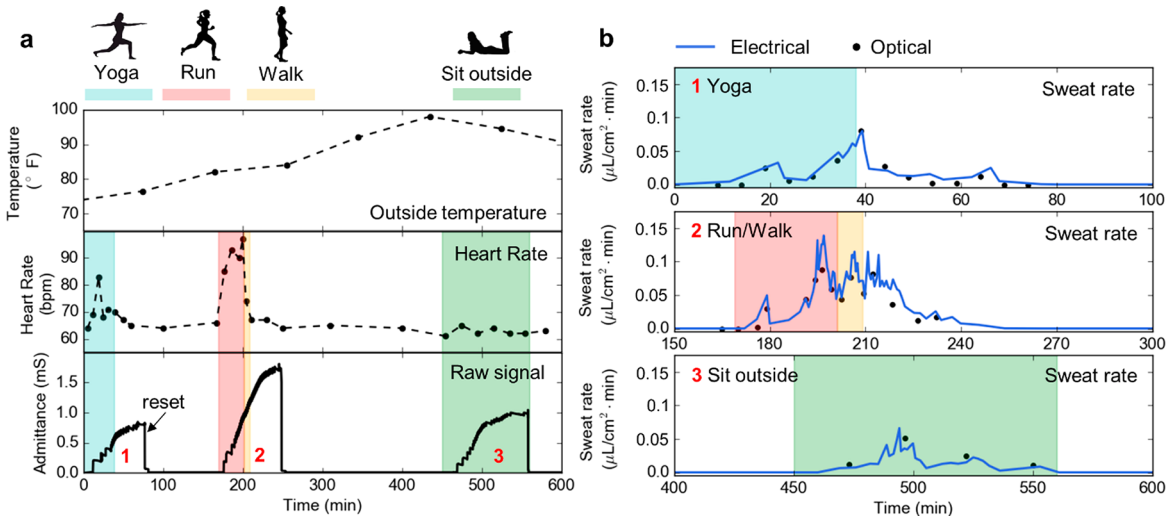

Figure 4. Ten hour multiactivity sweat rate monitoring using a 14 cm^2 collection area. (a) The subject spent a few hours doing sweat-inducing activities and the remainder of the time resting indoors. (b) Each period of activity—yoga, running, walking, and sitting outdoors in the heat—is shown in detail with comparison between optical and electrical flow rate measurements.

measurements to resume. In our device, a manually activated reset button behaves as a pressure pump to reset the channel using a negative or positive pressure mechanism, as shown in Figure 3a and SI Figure 4a, respectively. The reset button is a custom-molded PDMS suction cup that forms a seal over the air exchange pore in the electrode layer. The reset process begins after the channel has been filled to capacity and admittance gradually stepped up to a maximum. Both reset configurations are designed with an air exchange hole in addition to a sweat exit hole. For the negative pressure reset, the first step is to depress the reset button, which is located over the outlet of the channel. The pressurized air vents through the air exchange pore located just before the outlet, to ensure sweat is not pushed backward into the device. Then, the user blocks the air exchange pore with a finger while releasing the reset button. This draws sweat out of the channel and into the region under the button, where an absorptive pad serves as a waste reservoir. The channel is left empty and ready to resume sweat rate measurements. For the positive pressure reset, the air exchange pore is located directly above the sweat inlet hole at the center of the spiral. This pore is capped with a polytetrafluoroethylene (PTFE) resin membrane that allows airflow, but its inherent hydrophobicity blocks fluid passage below 7 kPa (Nitto TEMISH). To reset the device, the button is pressed and held until complete fluid expulsion into the absorptive pad at the outlet. The reset process can be repeated multiple times, as shown in Figure 3b for the negative pressure mechanism and SI Figure 4b for the positive pressure mechanism. Note that in the initial fill, the device entry chamber and channel are not wetted and thus can create a different breakthrough pressure needed for sweat to start flowing into the channel compared to after a reset. Further, the suction reset expels fluid from the channel but not always from the initial, entry sweat accumulation area, causing a slightly longer fill time on the first fill as sweat first accumulates in this chamber.

Signal quality is consistent for multiple resets, maintaining a steady maximum admittance value and well-defined steps until around three to five resets, when droplets of residual sweat begin to accumulate in the channel. To improve surface uniformity of the laser-cut channel and promote continuous fluid flow for clean resets, the sidewalls of the channel can be functionalized with a hydroxyl-terminated self-assembled monolayer (SAM).[39] This was used for the channel layers in the positive pressure reset device to remedy possible roughness and hydrophobic residue left by the laser-cutting process. Figure 3b further shows how the sweat rate electrode admittance response recovers back to baseline levels and repeatably increases again each time sweat is withdrawn to allow new sweat to enter the device, emphasizing that this scheme represents an effective mechanism for realizing resettability. Both mechanisms are designed to enable rapid fluidic reset for prolonged, nearly uninterrupted sweat rate monitoring.

Multihour Sweat Rate Tracking On-Body. Resettability extends the capability to monitor sweat dynamics from a single 90 min activity to a full 10 h day, as shown in Figure 4. Continuous sweat rate monitoring on the forearm of a healthy subject clearly indicates variations in thermoregulatory sweating with exercise intensity and ambient temperature. During periods of low-intensity exercise (yoga), high-intensity exercise (running, walking), and sedentary activity at different temperatures, both sweat rate and heart rate are seen to vary accordingly. Sweat rate is measured electrically as detailed above, along with optical measurements for cross-verification using a device affixed to the forearm with medical-grade tape over a 14 cm^2 collection area, and heart rate is measured with a commercial fitness tracking device. During low-intensity exercise, sweat rate and heart rate of the subject reach a maximum of 0.08 $\mu L\ min^{-1}\ cm^{-2}$ and 84 bpm. Optical measurements of sweat rate correlate well with device measurements, as seen in Figure 4b. As expected, sweat rates remain elevated for a cool-down period of some 40−60 min after the subject stops exercising. After a device reset and period of subject inactivity, an elevated sweat rate peaking at 0.15 $\mu L\ min^{-1}\ cm^{-2}$ along with heart rate at 98 bpm are measured during high-intensity exercise. Note that the device may be reset before completely full with no ill effect on sweat rate measurement, but the maximum admittance for that fill will be lower, as shown in this reset. Maximum admittance also varies with sweat ion content, but again with no bearing on sweat rate accuracy. Finally, after another reset and period of

https://doi.org/10.1021/acssensors.2c00177
ACS Sens. 2022, 7, 1156−1164

inactivity, the subject spent nearly 2 h sitting outdoors at the hottest time of day, while the temperature ranged from 32 to 38 °C. While the subject's heart rate remained at resting levels around 65 bpm during this sedentary activity, their sweat rate clearly increases to a maximum of 0.06 μL min^{-1} cm^{-2} in accordance with the body's thermoregulatory response. Continuous monitoring of sweat rate in combination with heart rate clearly and distinctly indicate both exercise- and heat-induced physiological strain. Due to the lack of gold-standard sweat rate measurement methods, this consideration of whether sweat rate measurements correlate as expected against physiological and behavioral events serves to validate the sensor response. The measured sweat secretion rate is consistently elevated during levels of activity associated with higher-than-baseline heart rate, compared to periods of rest. In this way, resting periods serve as a quasi-control and create confidence in the relative rate changes being conveyed. Going forward, the absolute accuracy can be verified by comparing sensor measurements against gravimetry in carefully controlled lab environments to limit the error of the latter.

Moving on to Figure 5, we are also able to capture rapid changes in sweat dynamics correlating with exercise intensity

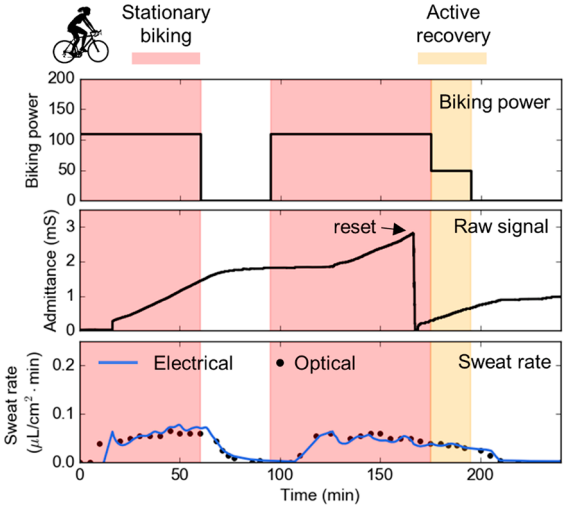

Figure 5. Impact of recovery on sweat rate during stationary biking using a 14 cm^2 collection area. The subject's sweat rate reflects the intensity of exercise. During the periods of cycling exercise (pink) sweat rate hovers around 0.05 μL min^{-1} cm^{-2}, with lower sweat rates during active recovery (yellow) consisting of continued cycling at a slower pace, and lowest sweat rates during rest (white).

of varying power output on a stationary bicycle, on the order of tens of minutes. A healthy subject cycled for 4 h with five periods including high-power cycling, low-power cycling, and rest. During high-power cycling, the subject's sweat rate averaged 0.05 μL min^{-1} cm^{-2}, whereas during the resting period, after equilibrating, sweat rate was negligible at the given resolution. After completing the first segment of high-power cycling, the subject rested for 40 min, during which the sweat rate slowly fell to a negligible value. During the second segment of high-power cycling, the device reached capacity and was reset, followed by the continuation of flow rate measurements, which began again near 0.05 μL min^{-1} cm^{-2}, as measured in the previous cycling period. This data set demonstrates the capability to reset the device midexercise and maintain expected flow rate measurements.

Finally, in Figure 6, we demonstrate the use of the sweat sensing patch for wireless monitoring of elevated-temperature

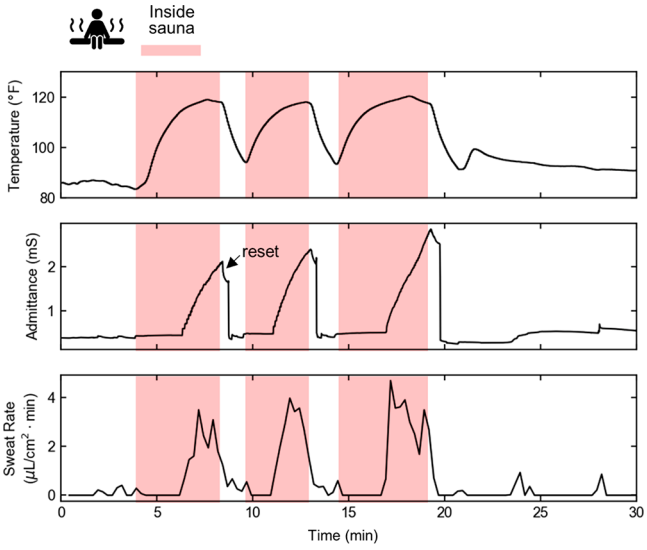

Figure 6. Thermally induced sedentary sweat monitoring using a 0.8 cm^2 collection area. The subject's sweat rate rises to 2−4 μL min^{-1} cm^{-2} during periods in the sauna, and at the end of each period the subject exits the sauna to reset the device. For this experiment, after conversion of admittance to device fill volume, the fill volume was downsampled at a rate of 1/15 before calculating the flow rate.

thermoregulatory sweating. A healthy subject wore the microfluidic sensing patch connected to the flexible, wireless readout board inside an electric sauna (~60 °C, ~40% RH) for three ~5 min periods. An ~0.8 cm^2 sweat collection area on the left forearm was defined by a region cut from medical tape (3 M 1577) used for adhesion of the patch to skin, and the board reported impedance measurements via Bluetooth Low Energy to a custom application on a mobile phone situated outside the sauna. A sensor on the board also monitored the temperature of the subject's environment. The board was encapsulated in polyethylene film sealed with polyimide tape to prevent moisture damage, insulating the sensor such that the measured temperature trend is accurate, but deviates from true ambient air temperature. At the start of the trial, the subject was actively sweating from prior acclimation inside the sauna. The measurements demonstrate that the subject maintains a 2−4 μL min^{-1} cm^{-2} sweat rate. Note that after a reset, there may be a brief measurement pause when fluid has been expelled from the collection area, as was the case in this trial, because it takes a couple minutes to refill the dead volume before sweat re-enters the measurement channel. However, this trial also demonstrates the robustness of the sweat rate sensor. After each reset and refilling period, the measurements resume nearly the same value, as expected for this sedentary activity and the controlled environment. This data set demonstrates functionality for monitoring sweat rate in high-temperature environments, when sweating becomes a critical bodily function for avoiding heatstroke as well as a risk factor for dehydration.[40]

Future iterations of the device could be designed for use beyond three to five resets for further prolonged measurement or use with subjects of higher sweat rate. There are several strategies that may extend device performance. When measurement failure occurs, it is typically via irregular filling

https://doi.org/10.1021/acssensors.2c00177
ACS Sens. 2022, 7, 1156−1164

due to sweat residue left along the channel walls that accumulates and disrupts fluid flow. After too many resets, this residue may wick incoming sweat along the sidewalls, blurring the admittance steps too much for digital readout or leaving the center of the channel empty and invalidating the measurement. Improving the uniformity and hydrophilicity of channel sidewalls would help with consistent fluid flow during expulsion as well as the following fills. While laser cutting, the technique utilized in this work, is a quick and precise method for channel fabrication, it is known to leave some debris and hydrophobic residue along the cut edge. An alternate tool like a cutting plotter may generate fewer nonuniformities.[9] Additionally, post-treatment with chemical SAM may be refined for greater coverage of the channel sidewalls. Finally, an approach to improve robustness of digital readout with varying flow profiles is to redesign the interdigitated electrodes with a smaller interaction area in order to keep the admittance steps sharp.

Hydrophilic channel walls are especially important because the measurement consistency between device fills can be affected by varying capillary forces. In the absence of fluid wicking, a dry, hydrophobic channel may present significant hydrodynamic resistance to sweat flow, especially if generating gland pressure is low. However, if the channel is hydrophilic due to chemical treatment or residue left by a prior filling, capillary action serves to enhance fluid uptake from the surface of the skin and lower the resistance to fluid flow through the channel. Two ways that our device has been engineered for low hydrodynamic resistance for accurate flow rate measurements are (1) design of channel dimensions for low interference with the expected secretory pressures and flow rates of our desired application and (2) hydrophilic treatment on three of the four channel walls—hydrophilic material for the capping layer in addition to hydroxyl group SAM-treated sidewalls.

Further developments to the device could include a holding enclosure to fix the suction cup in place while still allowing it to depress and decompress for ease of actuation during on-body use. To increase the frequency at which discrete sweat rate measurements can be made, more interdigitated electrode gates can be patterned for the serpentine channel to cross over. The spacing between gates can be reduced in accordance with fabrication capabilities to increase the resolution of discrete sweat rate measurements. Ultimately, electronics and actuators can be included to automatically initiate sweat withdrawal periodically or once the channel is detected to be filled for fully automated resettability. This remains to be realized in future work.

CONCLUSION

There are few current sweat rate measurement methods that provide accurate, quantitative measurements with systems that are portable and can be easily integrated into routine activities. Color-changing dyes, humidity chambers, and gravimetric measurements involving weighing secreted sweat volumes are impractical for routine sweat rate analysis. While some wearable sweat rate sensors have been presented in recent years, they too have limitations—namely, they suffer from interference from sweat's ionic composition, and they have small volume capacities that limit sweat rate measurement to short intervals of time. The device presented here overcomes these challenges as it uses a discrete impedimetric sensing scheme immune to interference from ionic concentration fluctuations and has an integrated resetting functionality that enables continuous measurement over prolonged periods. These are crucial advantages to making sweat rate monitoring continuous, routine, and unintrusive for daily measurement. Going forward, further work is needed to preserve signal integrity over even more reset cycles and to lower device-to-device variability to promote these devices out of the lab setting for real-world use.

Further, more subject studies should be done at scale to more deeply correlate physiological conditions with sweat rate and complementing biomarker concentrations. Simultaneous measurements of biomarker concentrations and sweat rate could be performed with the electrochemical sensing electrodes present in but unused by the device in this work. To begin, sweat rate and electrolyte concentrations should be studied alongside hydration status toward identifying, predicting, and even preventing dehydration.

EXPERIMENTAL SECTION

High-Throughput Fabrication of Sensing Patch. To produce sensing electrodes, a roll of polyethylene terephthalate (PET) substrate (Melinex ST506, 125 μm thick) was thermally pretreated (oven at 140 °C, 5 m/min, dwell time ∼0.7 min) before sequential roll-to-roll rotary silk screen printing of (i) silver conductive tracks (Asahi LS-411AW, oven-dried at 140 °C, 2 m/min, drying time ∼3 min), (ii) carbon electrodes (Loctite EDAG PF-407A, oven-dried at 120 °C, 4 m/min, drying time ∼1.8 min), (iii) two dielectric layers (Loctite EDAG 452SS, UV cured, 4 m/min,), and (iv) upper silver electrodes (Asahi LS-411AW, oven-dried at 140 °C, 2 m/min, drying time ∼3 min). Printed layers were manually registered, with the alignment monitored using a camera module mounted on the printing line. Laser (ELAS laser system with Ekspla Atlantic, DPL 015 3 UV laser) patterned electrode sheets, channel-defining double-sided microfluidic adhesive tape (3M 9965) and polyester cover film (3M 9984) were manually assembled to form the microfluidic sensing patch.

For more uniform fluid flow, the sidewalls of the laser-cut channel can be functionalized with a hydrophilic hydroxyl-terminated self-assembled monolayer (SAM). In this process, the channel layer first underwent O_2 plasma treatment at a power of 90 W, at 0.2 mTorr for 2 min. Next, it was soaked in 0.25 wt % bis(2-hydroxyethyl)-(3-aminopropyl)-triethoxysilane, HEA (Gelest, Inc.) in anhydrous ethanol (>99.5%, Sigma-Aldrich) for 1 h, followed by a thorough rinse with anhydrous ethanol. Finally, the layer was dried at 60 °C for 10 min before assembly of the microfluidic sensing patch.

Conversion of Admittance to Flow Rate. Admittance steps representing gate crossings were identified with a Python script examining the magnitude of the admittance difference between sequential data points. Differences above an appropriate threshold were marked as gate crossings. This sequence of gate crossings was then converted to a fill volume profile over time using the known volumetric increment of a channel segment. Finally, a discrete flow rate measurement was generated by taking the discrete derivative of this fill volume profile.

Device Characterization. Controlled flow rate experiments were carried out using Harvard Apparatus PHD 2000 Syringe Pump. Electrical sweat rate data were collected using E4980AL precision LCR meter (Keysight Technologies).

On-Body Sweat Analysis. On-body human trials were carried out at the University of California, Berkeley in compliance with the human research protocol (CPHS 2014−08−6636) approved by the Berkeley Institutional Review Board (IRB). On-body experiments at VTT were approved by the Research Ethics Committee of VTT. Informed consent was obtained from the subjects before enrollment in the study. Before attachment of the microfluidic device, the skin of the sensing site was wiped with alcohol wipes. Subjects were permitted to wear comfortable clothing. For heart rate measurements, a Fitbit wristwatch fitness tracker (Fitbit Charge 3) was used. To define the collection area and affix the patch to the skin for the

https://doi.org/10.1021/acssensors.2c00177
ACS Sens. 2022, 7, 1156−1164

duration of the measurement, adhesive (Adhesive Research 93690 or 3M 1577) was applied on top of the patch. No skin irritation or device delamination from prolonged use of adhesive were found during the extended on-body trials, in accordance with manufacturers' ratings for 5+ days of use. For the stationary bike trial, the subject cycled on an electronically braked leg-cycle ergometer (Gold's Gym Cycle Trainer 290C). Optical sweat rate data were collected by periodically capturing direct overhead images of the microfluidic channel and measuring the position of the fluid front from the images in AutoCAD. Electrical sweat rate data were collected with the E4980AL LCR meter for multiactivity and stationary cycling experiments and with custom wireless readout system for sauna experiment (SI Figure S1). Wireless sweat rate monitoring was realized by adapting a device that was previously demonstrated for monitoring wound care[41] to measure impedance at 100 kHz in 1 s intervals by BLE streaming to a custom mobile phone application. Further details on the implementation of the wireless readout system are given in the Supporting Information (Figure S6). No difference in quality was observed between measurements made by the two systems. Ambient temperature and humidity were measured with a digital thermometer/hygrometer (AcuRite 01083M). Figures were plotted via Python Matplotlib and MATLAB.

■ ASSOCIATED CONTENT

Supporting Information

The Supporting Information is available free of charge at https://pubs.acs.org/doi/10.1021/acssensors.2c00177.

Additional details on device design, electronics, and measurement validation are included as Figures S1−S6 (PDF)

■ AUTHOR INFORMATION

Corresponding Author

Ali Javey − *Department of Electrical Engineering and Computer Sciences, University of California, Berkeley, California 94720, United States; Berkeley Sensor and Actuator Center, University of California, Berkeley, California 94720, United States; Materials Sciences Division, Lawrence Berkeley National Laboratory, Berkeley, California 94720, United States;* orcid.org/0000-0001-7214-7931; Email: ajavey@berkeley.edu

Authors

Mallika Bariya − *Department of Electrical Engineering and Computer Sciences, University of California, Berkeley, California 94720, United States; Berkeley Sensor and Actuator Center, University of California, Berkeley, California 94720, United States; Materials Sciences Division, Lawrence Berkeley National Laboratory, Berkeley, California 94720, United States;* orcid.org/0000-0002-3416-8157

Noelle Davis − *Department of Electrical Engineering and Computer Sciences, University of California, Berkeley, California 94720, United States; Berkeley Sensor and Actuator Center, University of California, Berkeley, California 94720, United States; Materials Sciences Division, Lawrence Berkeley National Laboratory, Berkeley, California 94720, United States;* orcid.org/0000-0001-7198-4578

Liam Gillan − *VTT Technical Research Centre of Finland Ltd, Espoo 02150, Finland;* orcid.org/0000-0002-0692-1359

Elina Jansson − *VTT Technical Research Centre of Finland Ltd, Oulu 90570, Finland*

Annukka Kokkonen − *VTT Technical Research Centre of Finland Ltd, Oulu 90570, Finland*

Colm McCaffrey − *VTT Technical Research Centre of Finland Ltd, Espoo 02150, Finland*

Jussi Hiltunen − *VTT Technical Research Centre of Finland Ltd, Oulu 90570, Finland*

Complete contact information is available at: https://pubs.acs.org/10.1021/acssensors.2c00177

Author Contributions

#M.B. and N.D. contributed equally to this work. M.B., L.G., N.D., and A.J. conceived the idea and designed the experiments. C.M.C. designed the readout electronics, L.G., E.J., A.K., and J.H. contributed the manufacture of the microfluidic devices. M.B., N.D., and L.G. performed tests on sensors and human studies.

Notes

The authors declare no competing financial interest.

■ ACKNOWLEDGMENTS

This work was supported by the Berkeley Sensors and Actuators Center (BSAC) and the Bakar Fellowship. Part of the facilities at VTT were funded by the Academy of Finland Research Infrastructure "Printed Intelligence Infrastructure" (PII-FIRI, grant no. 320020). N.D. acknowledges support from the National Defense Science & Engineering Graduate (NDSEG) Fellowship Program. The authors would like to thank Jonghwa Park for assistance with device fabrication, Mohini Bariya for drawing of illustrations, Christina Liedert for coordination of VTT pilot line facilities, Jari Rekilä for technical assistance with printing and laser designs, and Marko Korkalainen for assisting development of the wireless readout system.

■ REFERENCES

(1) Baker, L. B.; Ungaro, C. T.; Sopeña, B. C.; Nuccio, R. P.; Reimel, A. J.; Carter, J. M.; Stofan, J. R.; Barnes, K. A. Body Map of Regional vs. Whole Body Sweating Rate and Sweat Electrolyte Concentrations in Men and Women during Moderate Exercise-Heat Stress. *J. Appl. Physiol.* **2018**, *124* (5), 1304−1318.

(2) Foster, K. G.; Hey, E. N.; O'Connell, B. Sweat Function in Babies with Defects of the Central Nervous System. *Dev. Med. Child Neurol.* **1969**, *11*, 94−94.

(3) Baker, L. B. Physiology of Sweat Gland Function: The Roles of Sweating and Sweat Composition in Human Health. *Temp. Multidiscip. Biomed. J.* **2019**, *6* (3), 211−259.

(4) Patterson, M. J.; Galloway, S. D. R.; Nimmo, M. A. Variations in Regional Sweat Composition in Normal Human Males. *Exp. Physiol.* **2000**, *85* (6), 869−875.

(5) Sonner, Z.; Wilder, E.; Heikenfeld, J.; Kasting, G.; Beyette, F.; Swaile, D.; Sherman, F.; Joyce, J.; Hagen, J.; Kelley-Loughnane, N.; Naik, R. The Microfluidics of the Eccrine Sweat Gland, Including Biomarker Partitioning, Transport, and Biosensing Implications. *Biomicrofluidics* **2015**, *9* (3), 031301.

(6) Gao, W.; Emaminejad, S.; Nyein, H. Y. Y.; Challa, S.; Chen, K.; Peck, A.; Fahad, H. M.; Ota, H.; Shiraki, H.; Kiriya, D.; Lien, D.-H.; Brooks, G. A.; Davis, R. W.; Javey, A. Fully Integrated Wearable Sensor Arrays for Multiplexed *in Situ* Perspiration Analysis. *Nature* **2016**, *529* (7587), 509.

(7) Jia, W.; Bandodkar, A. J.; Valdés-Ramírez, G.; Windmiller, J. R.; Yang, Z.; Ramírez, J.; Chan, G.; Wang, J. Electrochemical Tattoo Biosensors for Real-Time Noninvasive Lactate Monitoring in Human Perspiration. *Anal. Chem.* **2013**, *85* (14), 6553−6560.

(8) Koh, A.; Kang, D.; Xue, Y.; Lee, S.; Pielak, R. M.; Kim, J.; Hwang, T.; Min, S.; Banks, A.; Bastien, P.; Manco, M. C.; Wang, L.; Ammann, K. R.; Jang, K.-I.; Won, P.; Han, S.; Ghaffari, R.; Paik, U.; Slepian, M. J.; Balooch, G.; Huang, Y.; Rogers, J. A. A Soft, Wearable Microfluidic Device for the Capture, Storage, and Colorimetric

Sensing of Sweat. *Sci. Transl. Med.* **2016**, *8* (366), 366ra165−366ra165.
(9) Alizadeh, A.; Burns, A.; Lenigk, R.; Gettings, R.; Ashe, J.; Porter, A.; McCaul, M.; Barrett, R.; Diamond, D.; White, P.; Skeath, P.; Tomczak, M. A Wearable Patch for Continuous Monitoring of Sweat Electrolytes during Exertion. *Lab. Chip* **2018**, *18* (17), 2632−2641.
(10) Rose, D. P.; Ratterman, M. E.; Griffin, D. K.; Hou, L.; Kelley-Loughnane, N.; Naik, R. R.; Hagen, J. A.; Papautsky, I.; Heikenfeld, J. C. Adhesive RFID Sensor Patch for Monitoring of Sweat Electrolytes. *IEEE Trans. Biomed. Eng.* **2015**, *62* (6), 1457−1465.
(11) Lee, H.; Song, C.; Hong, Y. S.; Kim, M. S.; Cho, H. R.; Kang, T.; Shin, K.; Choi, S. H.; Hyeon, T.; Kim, D.-H. Wearable/Disposable Sweat-Based Glucose Monitoring Device with Multistage Transdermal Drug Delivery Module. *Sci. Adv.* **2017**, *3* (3), No. e1601314.
(12) Bariya, M.; Li, L.; Ghattamaneni, R.; Ahn, C. H.; Nyein, H. Y. Y.; Tai, L.-C.; Javey, A. Glove-Based Sensors for Multimodal Monitoring of Natural Sweat. *Sci. Adv.* **2020**, *6* (35), No. eabb8308.
(13) Lin, Y.; Bariya, M.; Javey, A. Wearable Biosensors for Body Computing. *Adv. Funct. Mater.* **2021**, *31* (39), 2008087.
(14) Tai, L.-C.; Gao, W.; Chao, M.; Bariya, M.; Ngo, Q. P.; Shahpar, Z.; Nyein, H. Y. Y.; Park, H.; Sun, J.; Jung, Y.; Wu, E.; Fahad, H. M.; Lien, D.-H.; Ota, H.; Cho, G.; Javey, A. Methylxanthine Drug Monitoring with Wearable Sweat Sensors. *Adv. Mater.* **2018**, *30* (23), 1707442.
(15) Zhao, J.; Nyein, H. Y. Y.; Hou, L.; Lin, Y.; Bariya, M.; Ahn, C. H.; Ji, W.; Fan, Z.; Javey, A. A Wearable Nutrition Tracker. *Adv. Mater.* **2021**, *33* (1), 2006444.
(16) Morris, D.; Coyle, S.; Wu, Y.; Lau, K. T.; Wallace, G.; Diamond, D. Bio-Sensing Textile Based Patch with Integrated Optical Detection System for Sweat Monitoring. *Sens. Actuators B Chem.* **2009**, *139* (1), 231−236.
(17) Emaminejad, S.; Gao, W.; Wu, E.; Davies, Z. A.; Nyein, H. Y. Y.; Challa, S.; Ryan, S. P.; Fahad, H. M.; Chen, K.; Shahpar, Z.; Talebi, S.; Milla, C.; Javey, A.; Davis, R. W. Autonomous Sweat Extraction and Analysis Applied to Cystic Fibrosis and Glucose Monitoring Using a Fully Integrated Wearable Platform. *Proc. Natl. Acad. Sci. U. S. A.* **2017**, *114* (18), 4625−4630.
(18) Abellán-Llobregat, A.; Jeerapan, I.; Bandodkar, A.; Vidal, L.; Canals, A.; Wang, J.; Morallón, E. A Stretchable and Screen-Printed Electrochemical Sensor for Glucose Determination in Human Perspiration. *Biosens. Bioelectron.* **2017**, *91*, 885−891.
(19) Korpelainen, J. T.; Sotaniemi, K. A.; Myllylä, V. V. Autonomic Nervous System Disorders in Stroke. *Clin. Auton. Res.* **1999**, *9* (6), 325−333.
(20) Kamei, T.; Tsuda, T.; Kitagawa, S.; Naitoh, K.; Nakashima, K.; Ohhashi, T. Physical Stimuli and Emotional Stress-Induced Sweat Secretions in the Human Palm and Forehead. *Anal. Chim. Acta* **1998**, *365* (1−3), 319−326.
(21) Aver, D. H.; Shah, S. H.; Eder, D. N.; Wildschindtz, G. Nocturnal Sweating and Temperature in Depression. *Acta Psychiatr. Scand.* **1999**, *100* (4), 295−301.
(22) Randall, W. C.; Peiss, C. N. The Relationship Between Skin Hydration and the Suppression of Sweating1. *J. Invest. Dermatol.* **1957**, *28* (6), 435−441.
(23) Oppliger, R. A.; Bartok, C. Hydration Testing of Athletes. *Sports Med.* **2002**, *32* (15), 959−971.
(24) Baker, L. B.; Model, J. B.; Barnes, K. A.; Anderson, M. L.; Lee, S. P.; Lee, K. A.; Brown, S. D.; Reimel, A. J.; Roberts, T. J.; Nuccio, R. P.; Bonsignore, J. L.; Ungaro, C. T.; Carter, J. M.; Li, W.; Seib, M. S.; Reeder, J. T.; Aranyosi, A. J.; Rogers, J. A.; Ghaffari, R. Skin-Interfaced Microfluidic System with Personalized Sweating Rate and Sweat Chloride Analytics for Sports Science Applications. *Sci. Adv.* **2020**, *6* (50), No. eabe3929.
(25) Nyein, H. Y. Y.; Bariya, M.; Kivimäki, L.; Uusitalo, S.; Liaw, T. S.; Jansson, E.; Ahn, C. H.; Hangasky, J. A.; Zhao, J.; Lin, Y.; Happonen, T.; Chao, M.; Liedert, C.; Zhao, Y.; Tai, L.-C.; Hiltunen, J.; Javey, A. Regional and Correlative Sweat Analysis Using High-Throughput Microfluidic Sensing Patches toward Decoding Sweat. *Sci. Adv.* **2019**, *5* (8), No. eaaw9906.
(26) Kavouras, S. A. Assessing Hydration Status. *Curr. Opin. Clin. Nutr. Metab. Care* **2002**, *5* (5), 519−524.
(27) Shirreffs, S. M. Markers of Hydration Status. *J. Sports Med. Phys. Fitness* **2000**, *40* (1), 80−84.
(28) Taylor, N. A.; Machado-Moreira, C. A. Regional Variations in Transepidermal Water Loss, Eccrine Sweat Gland Density, Sweat Secretion Rates and Electrolyte Composition in Resting and Exercising Humans. *Extreme Physiol. Med.* **2013**, *2* (1), 4.
(29) Yokus, M. A.; Agcayazi, T.; Traenkle, M.; Bozkurt, A.; Daniele, M. A. Wearable Sweat Rate Sensors. *2020 IEEE SENSORS* **2020**, 1−4, DOI: 10.1109/SENSORS47125.2020.9278818.
(30) Yuan, Z.; Hou, L.; Bariya, M.; Nyein, H. Y. Y.; Tai, L.-C.; Ji, W.; Li, L.; Javey, A. A Multi-Modal Sweat Sensing Patch for Cross-Verification of Sweat Rate, Total Ionic Charge, and Na+ Concentration. *Lab. Chip* **2019**, *19* (19), 3179−3189.
(31) Nyein, H. Y. Y.; Bariya, M.; Tran, B.; Ahn, C. H.; Brown, B. J.; Ji, W.; Davis, N.; Javey, A. A Wearable Patch for Continuous Analysis of Thermoregulatory Sweat at Rest. *Nat. Commun.* **2021**, *12* (1), 1823.
(32) Jain, V.; Ochoa, M.; Jiang, H.; Rahimi, R.; Ziaie, B. A Mass-Customizable Dermal Patch with Discrete Colorimetric Indicators for Personalized Sweat Rate Quantification. *Microsyst. Nanoeng.* **2019**, *5* (1), 1−12.
(33) Reeder, J. T.; Xue, Y.; Franklin, D.; Deng, Y.; Choi, J.; Prado, O.; Kim, R.; Liu, C.; Hanson, J.; Ciraldo, J.; Bandodkar, A. J.; Krishnan, S.; Johnson, A.; Patnaude, E.; Avila, R.; Huang, Y.; Rogers, J. A. Resettable Skin Interfaced Microfluidic Sweat Collection Devices with Chemesthetic Hydration Feedback. *Nat. Commun.* **2019**, *10* (1), 5513.
(34) Zhou, Y.; Han, H.; Naw, H. P. P.; Lammy, A. V.; Goh, C. H.; Boujday, S.; Steele, T. W. J. Real-Time Colorimetric Hydration Sensor for Sport Activities. *Mater. Des.* **2016**, *90*, 1181−1185.
(35) Choi, D.-H.; Gonzales, M.; Kitchen, G. B.; Phan, D.-T.; Searson, P. C. A Capacitive Sweat Rate Sensor for Continuous and Real-Time Monitoring of Sweat Loss. *ACS Sens.* **2020**, *5* (12), 3821−3826.
(36) Bariya, M.; Shahpar, Z.; Park, H.; Sun, J.; Jung, Y.; Gao, W.; Nyein, H. Y. Y.; Liaw, T. S.; Tai, L.-C.; Ngo, Q. P.; Chao, M.; Zhao, Y.; Hettick, M.; Cho, G.; Javey, A. Roll-to-Roll Gravure Printed Electrochemical Sensors for Wearable and Medical Devices. *ACS Nano* **2018**, *12* (7), 6978−6987.
(37) Liedert, C.; Rannaste, L.; Kokkonen, A.; Huttunen, O.-H.; Liedert, R.; Hiltunen, J.; Hakalahti, L. Roll-to-Roll Manufacturing of Integrated Immunodetection Sensors. *ACS Sens.* **2020**, *5* (7), 2010−2017.
(38) Pirovano, P.; Dorrian, M.; Shinde, A.; Donohoe, A.; Brady, A. J.; Moyna, N. M.; Wallace, G.; Diamond, D.; McCaul, M. A Wearable Sensor for the Detection of Sodium and Potassium in Human Sweat during Exercise. *Talanta* **2020**, *219*, 121145.
(39) Yerushalmi, R.; Ho, J. C.; Jacobson, Z. A.; Javey, A. Generic Nanomaterial Positioning by Carrier and Stationary Phase Design. *Nano Lett.* **2007**, *7* (9), 2764−2768.
(40) Bouchama, A.; Knochel, J. P. Heat Stroke. *N. Engl. J. Med.* **2002**, *346* (25), 1978−1988.
(41) Mc Caffrey, C.; Flak, J.; Kiri, K.; Pursula, P. Flexible Bioimpedance Spectroscopy System for Wound Care Monitoring. In *2019 IEEE Biomedical Circuits and Systems Conference (BioCAS)*; 2019; pp 1−4. DOI: 10.1109/BIOCAS.2019.8919095.